Article

# Charge Stability and Charge-State-Based Spin Readout of Shallow Nitrogen-Vacancy Centers in Diamond

Rakshyakar Giri,* Rasmus Høy Jensen, Deepak Khurana, Juanita Bocquel, Ilya P. Radko, Johannes Lang, Christian Osterkamp, Fedor Jelezko, Kirstine Berg-Sørensen, Ulrik L. Andersen, and Alexander Huck*

Cite This: ACS Appl. Electron. Mater. 2023, 5, 6603−6610

Read Online

ACCESS | Metrics & More | Article Recommendations | SI Supporting Information

**ABSTRACT:** Spin-based applications of the negatively charged nitrogen-vacancy (NV) center in diamonds require an efficient spin readout. One approach is the spin-to-charge conversion (SCC), relying on mapping the spin states onto the neutral ($NV^0$) and negative ($NV^-$) charge states followed by a subsequent charge readout. With high charge-state stability, SCC enables extended measurement times, increasing precision and minimizing noise in the readout compared to the commonly used fluorescence detection. Nanoscale sensing applications, however, require shallow NV centers within a few nanometers distance from the surface where surface related effects might degrade the NV charge state. In this article, we investigate the charge state initialization and stability of single NV centers implanted ≈5 nm below the surface of a flat diamond plate. We demonstrate the SCC protocol on four shallow NV centers suitable for nanoscale sensing, obtaining a reduced readout noise of 5−6 times the spin-projection noise limit. We investigate the general applicability of the SCC for shallow NV centers and observe a correlation between the NV charge-state stability and readout noise. Coating the diamond with glycerol improves both the charge initialization and stability. Our results reveal the influence of the surface-related charge environment on the NV charge properties and motivate further investigations to functionalize the diamond surface with glycerol or other materials for charge-state stabilization and efficient spin-state readout of shallow NV centers suitable for nanoscale sensing.

**KEYWORDS:** shallow NV centers, spin-to-charge conversion, charge-state dynamics, glycerol coating, surface effects
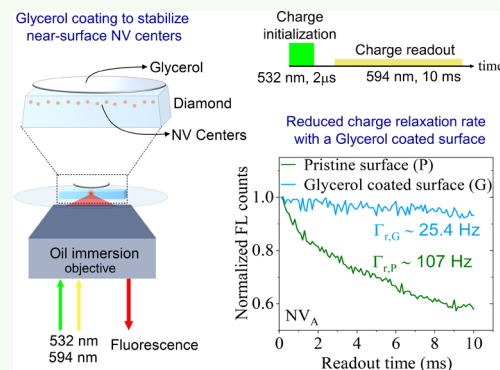
## INTRODUCTION

The negatively charged nitrogen-vacancy ($NV^-$) center in diamond has excellent spin properties at room temperature with a long lifetime and coherence, enabling a broad range of applications. These include the sensing of magnetic and electric fields with high sensitivity and nanometer-scale spatial resolution.[1−3] Central to any $NV^-$ center sensing task is the ability to initialize and read out the spin state optically. The most common approach to read out the spin state is via the fluorescence rate, enabled by spin-dependent intersystem crossing from the triplet excited to a singlet state.[4] The intersystem crossing mechanism sets a lower limit on the spin readout duration to around 300 ns as determined by the singlet-state lifetime[5] that together with low photon counts in the order of 0.1 per readout hinders the efficient measurement of the spin state. In the context of sensing, it is thus required to repeat the scheme multiple times in order to build up sufficient photon statistics to determine the spin state.[5,6] Nanopillars[7] or solid immersion lenses[8] might be used to increase the photon collection efficiency and improve the readout signal-to-noise ratio (SNR), but yet the attainable photon count rates are not sufficient to measure the spin state in a single shot.

In addition to photoelectrical readout,[9] another approach for spin readout involves the charge degree of freedom of the NV center that in addition to $NV^-$ may also exist in the neutral charge state $NV^0$. Deep in the bulk, the charge state ratio between the two is highly stable in the dark or under weak optical excitation.[10−12] With zero-phonon lines at 575 and 637 nm for $NV^0$ and $NV^-$, respectively, and therefore different absorption spectra, the charge states are distinguishable via selective illumination that excites $NV^-$ but not $NV^{0}$.[13] In the spin-to-charge conversion (SCC) protocol,[14] population of the $m_s = 0$ spin state is transferred to $NV^0$ via a photoionization process,[13,15] while the population of the $m_s = \pm 1$ spin state remains in the $NV^-$ charge state. The subsequent charge-state readout may be long and efficient provided sufficient photon counts and charge-state stability are attained within the readout duration. Using this approach, >1 photon per readout
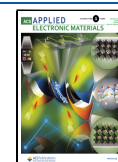
may be detected when the system is in $m_s = \pm 1$, significantly increasing SNR per readout at the cost of significantly increased integration time as compared to standard fluorescence detection.

Applying the SCC protocol to an NV center in a diamond nanobeam with significantly improved photon collection efficiency compared to bulk diamond, Shields et al.[14] demonstrated an SNR $\approx 0.55$ per readout corresponding to a noise factor of $\approx 3\sigma_p$, where $\sigma_p$ is the spin-projection noise limit.[16] More recently, the SCC readout has been demonstrated for NV center ensembles in nanodiamonds[17] and bulk diamonds,[18] and for single NV centers deep in the bulk,[19] and applied in covariance magnetometry.[20] Nanoscale sensing tasks including nuclear magnetic resonance (NMR)[21,22] or sensing of free radicals,[23] however, require single NV centers within a few nanometers from the diamond surface where the sensing signal is sufficiently strong.[24] In the vicinity of the surface, effects including upward energy band bending[25] and electron tunneling to nearby surface traps[11] are known to cause ionization of NV$^-$ to NV$^0$ at rates on the order of the inverse readout time or even faster. Although it has been demonstrated that SCC can work for NV centers implanted within a few nanometers from the surface in diamond nanopillars,[26] the general applicability of the SCC protocol to near-surface NV centers as well as the possible detrimental impact of surface-related effects remains unexplored as of yet.

In this article, we explore the charge-state stability and the SCC protocol on single NV centers implanted $\approx 5$ nm below the surface of a flat diamond plate. The implanted side of the diamond is accessible to apply a solution bath or nano-objects, an experimental configuration relevant for nanoscale sensing and spin mechanical coupling. We use a simplified experimental approach with only two lasers: one at 532 nm for NV charge and spin initialization and another at 594 nm for spin-state selective ionization and charge-state readout. From the detailed characterization of 33 single NV centers, we observe a strong variability of the probability to initialize into NV$^-$. We present data of four NV centers labeled NV$_A$–NV$_D$ that are representative of the distribution. We show that after coating the diamond with deuterated glycerol, the initialization probability into NV$^-$ increases while simultaneously the ionization rate from NV$^-$ to NV$^0$ decreases as compared to the pristine surface. Furthermore, we demonstrate the general applicability of the SCC protocol on four near-surface NV centers. Our investigations indicate the importance of the local charge environment for the NV charge-state stability as well as the overall performance of the SCC protocol. We obtain a noise level as low as $\approx 5\sigma_p$ corresponding to a single-shot SNR $\approx 0.3$, a result comparable to that obtained with NV centers in the bulk or nanostructures with higher attainable photon count rates.

## EXPERIMENTAL METHODS

All measurements reported in this article were conducted on a 50 $\mu$m thin electronic-grade diamond plate (Element Six) with (100) surface orientation. The sample was overgrown with a 100 nm thick and $^{12}$C-enriched (<0.05% $^{13}$C) layer of diamond using chemical vapor deposition. NV centers were created via implantation of $^{15}$N$^+$ ions with an energy of 2.5 keV and a dose of $5 \times 10^8$ cm$^{-2}$ (process pressure $<1 \times 10^{-7}$ mbar).[27] Subsequent annealing in an ultrahigh vacuum at 1000 °C for 3 h heals radiation damage due to the ion bombardment, mobilizes vacancies, and, through capture of an implanted nitrogen, yields a Gaussian-like distribution of single NV centers with a mean depth $\approx 5$ nm below the surface. The diamond

was cleaned in a boiling acid mixture consisting in equal parts of nitric, perchloric, and sulfuric acid (triacid cleaning) to remove surface contaminants[28] and creating a hydrophilic surface with partial oxygen termination.[29,30] With these near-surface NV centers and using a Hahn-echo sequence, we measured $T_2$ coherence times in the range from 3 to 15 $\mu$s, in good agreement with values obtained for a different sample fabricated using the same equipment and process parameters.[31]

We used a home-built scanning confocal microscope setup with an NA = 1.4 immersion-oil objective to investigate the NV charge state and implement the SCC protocol. The power of each laser, 532 and 594 nm, was controlled using acousto-optic modulators in a double-pass configuration to generate pulses for charge and spin initialization, shelving, ionization, and readout. After long-pass filtering with a cut-on at 650 nm, the NV fluorescence signal was detected with a single-photon-sensitive avalanche photodiode with dark counts <200 per second. Together with the selective excitation at 594 nm, this configuration ensures, to a very high degree, that the signal stems from the NV$^-$ emission. With a motorized 3-axis translation stage, we controlled the position of a permanent magnet to produce a bias magnetic field of $\approx 7$ mT along one of the four [111] crystal axes that all NV centers investigated here are aligned along. The diamond plate was horizontally mounted on a 170 $\mu$m thick cover glass with the NV layer on the top side, exposed to either air or solution and suitable for nanoscale sensing (Figure 1a). The excitation lasers pass from below through the cover glass and the diamond, and the fluorescence is collected from the same side (Supporting Information). Measurements on all the NV centers with a pristine surface and with a glycerol-coated surface were performed without removing the diamond sample from the setup. To passivate the diamond surface, we carefully put a small droplet of deuterated glycerol (glycerol-$d_8$ from Sigma-Aldrich) with a micropipette at the amount sufficient to cover the investigated region of diamond. No special procedure has been used to ensure spreading of glycerol through the surface, so the thickness of the layer was given by the glycerol surface tension and was of the order of 100 $\mu$m.

## RESULTS

**Charge-State Initialization and Stability.** We begin our investigations by characterizing the charge states of 33 near-surface NV centers by applying the protocol illustrated in Figure 1b. The 2 $\mu$s short 532 nm pulse (power $\approx 400$ $\mu$W; all laser powers specified herein are measured at the entrance to the objective) has the purpose to initialize the NV center into NV$^-$, followed by a weak 10 ms long 594 nm pulse (power $\approx 3.5$ $\mu$W) to selectively read out the charge state. The 594 nm readout laser mainly excites NV$^-$ as illustrated on the energy level diagrams in Figure 1c, which leads to a charge-state-dependent fluorescence intensity. During the readout, the NV center can ionize from NV$^-$ to NV$^0$ and recombine from NV$^0$ to NV$^-$ with the rates $\Gamma^{-0}$ and $\Gamma^{0-}$, respectively. The charge-state switching rates increase with increasing optical excitation power. The stability of the normalized fluorescence intensity during a readout pulse for NV$_A$ is shown in Figure 1d. The photon-number distribution $P(n)$ obtained from NV$_A$ with the pristine diamond surface is plotted in Figure 1e, where the gray- and red-shaded areas illustrate the contributions of NV$^0$ and NV$^-$, respectively. We fitted the temporal evolution of $P(n)$ with a model[11,14,32] (100 $\mu$s resolution) to extract the photon detection rates $\gamma^0$ and $\gamma^-$ from NV$^0$ and NV$^-$, respectively, as well as $\Gamma^{-0}$, $\Gamma^{0-}$, and the NV$^-$ population $P_0(\text{NV}^-)$ at the start of the readout pulse. With the pristine diamond surface, we obtain $P_0(\text{NV}^-) = 0.56$ and $\Gamma^{-0} = 101$ Hz, while $\Gamma^{0-} \approx 6$ Hz (note that due to a limited measurement time and a relatively high stability of the NV$^0$ charge state, it is not possible to quantify $\Gamma^{0-}$ with high accuracy within the
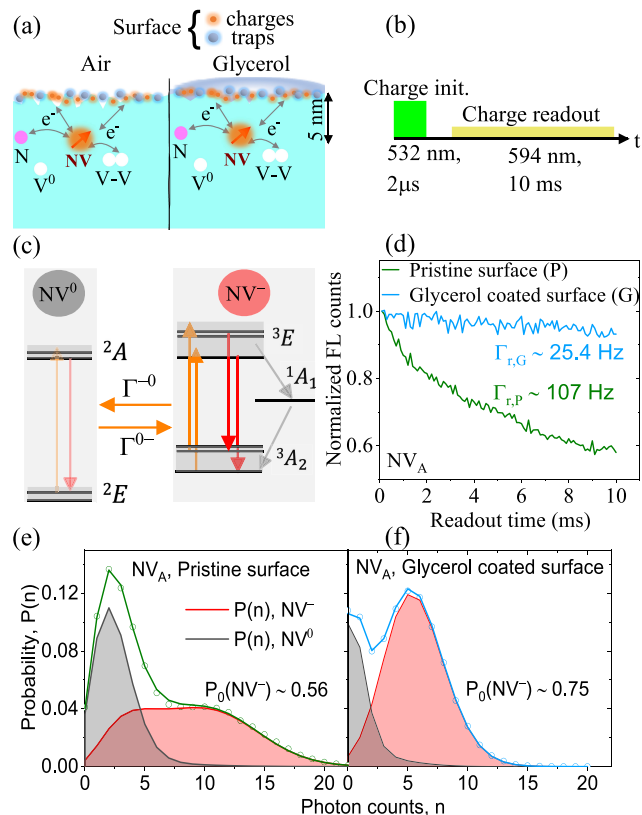
**Figure 1.** Surface-related effects and charge-state stability of shallow NV centers. (a) Illustration of ≈5 nm shallow NV centers and their interaction with the local charge environment with glycerol passivating surface charges and traps. (b) Pulse sequence to measure the NV⁻ charge-initialization probability $P_0(NV^-)$, applying 532 nm initialization and 594 nm readout pulses. (c) Illustration of the energy levels of NV⁰ and NV⁻ together with allowed transition rates. The 594 nm laser ideally excites only NV⁻. For strong excitation, it can ionize ($\Gamma^{-0}$) NV⁻ to NV⁰ and induce recombination ($\Gamma^{0-}$) from NV⁰ to NV⁻. The charge-state switching is suppressed for weak excitation, and the NV⁰ center remains dark under 594 nm excitation. (d) Fluorescence evolution of NV$_A$ during the readout pulse, showing a reduced relaxation rate after adding glycerol ($\Gamma_{r,G}$) as compared to the relaxation with the pristine surface ($\Gamma_{r,P}$). (e, f) Photon-number distribution $P(n)$ of NV$_A$ with the pristine (e) and the glycerol-coated (f) surface. The gray and red-shaded areas illustrate the respective contributions of NV⁰ and NV⁻.

measurement time). Afterward, we coated the diamond surface with glycerol, resulting in a significant change of $P(n)$ as presented in Figure 1f. The value of $P_0(NV^-)$ substantially increases to 0.75 and is now comparable to results from NV centers deeper in the bulk.[13,33] Furthermore, $\Gamma^{-0}$ substantially decreases to 9 Hz, demonstrating improved charge-state stability during the readout after coating the diamond surface with glycerol.

The increased charge-state stability of NV$_A$ after application of glycerol is also directly seen in the average fluorescence during the readout pulse as shown in Figure 1d. With the pristine surface, the fluorescence level reduces with a rate $\Gamma_{r,P} \approx \Gamma^{-0} + \Gamma^{0-} \approx 107$ Hz, while after application of glycerol the reduction is lower with a rate $\Gamma_{r,G} \approx 25$ Hz.

In Figure 2a, we plot the NV⁻ initialization probability $P_0(NV^-)$ versus the ionization rate $\Gamma^{-0}$ for 33 single NV centers both with the pristine diamond surface and after the application of glycerol. The histogram for $P_0(NV^-)$ is shown in



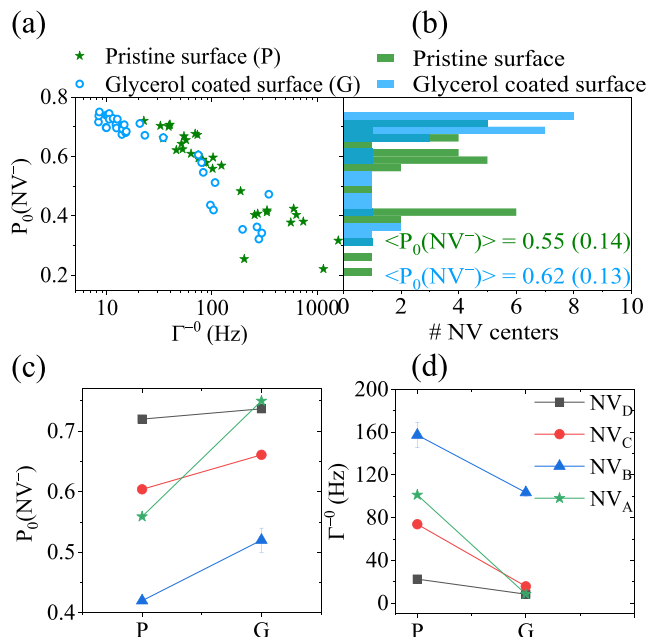**Figure 2.** (a) NV⁻ charge initialization probability $P_0(NV^-)$ versus ionization rate $\Gamma^{-0}$ for 33 NV centers with the pristine and the glycerol-coated surfaces. (b) Histogram of $P_0(NV^-)$. (c, d) Comparison of $P_0(NV^-)$ and $\Gamma^{-0}$ for pristine (P) and glycerol-coated (G) surface for emitters NV$_A$−NV$_D$.

Figure 2b. We observe an anticorrelation between $P_0(NV^-)$ and $\Gamma^{-0}$ irrespective of the surface condition. Upon the application of glycerol, $P_0(NV^-)$ increases for all NV centers (see Figure 2c for NV$_A$−NV$_D$) and correspondingly $\Gamma^{-0}$ reduces (see Figure 2d for NV$_A$−NV$_D$).

Our results show that the application of glycerol generally increases the charge-initialization probability of the ≈5 nm shallow NV centers into the NV⁻ state with a maximum probability ≈75% comparable to that of NV centers in the bulk. However, for some NV centers, including NV$_B$, the charge-initialization probability (ionization rate) remains low (high) and only marginally improves compared to the pristine surface.

**SCC Protocol.** In the next step, we implement the SCC protocol (Figure 3a) on four NV centers (NV$_A$−NV$_D$) that have different $P_0(NV^-)$, and we benchmark the performance of SCC by estimating the spin-readout noise $\sigma_R$.[14,16] Besides initialization into NV⁻, the initial 2 μs, 532 nm pulse (power ≈ 400 μW) also prepares the spin state into $m_s = 0$, which subsequently can be transferred to $m_s = -1$ with a $\pi$ pulse. The following short 594 nm pulse (power ≈ 4.4 mW) then likely shelves the NV⁻ center into the singlet state when in $m_s = -1$ or leaves the population in the triplet state with a higher probability when in $m_s = 0$. Applied immediately after the shelving pulse, the triplet state of the NV center is ionized with a 29 mW (maximum available) and a 594 nm pulse of duration $t_{ion}$, thus effectively mapping the NV center spin states onto the distribution of charge states. Finally, the charge state is read out using a weak 15 ms long (power 3.5 μW) 594 nm pulse. The optimal duration and power of each pulse have been determined separately (see the Supporting Information). As an example, in Figure 3b we plot the integrated photon counts $\alpha_{m_s}$ acquired during the first 2 ms readout window for the initial spin states $m_s = 0$ and $m_s = -1$ as a function of the ionization-
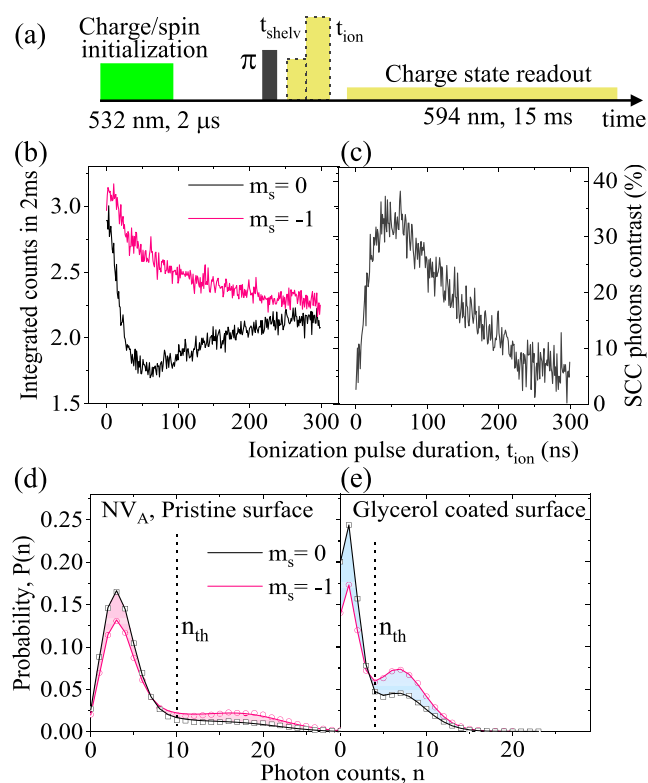
**Figure 3.** SCC protocol and effects of surface condition. (a) Illustration of the pulse sequence to implement the SCC protocol, where the height of the orange (594 nm) pulses indicates the strength. (b) Photon counts integrated in 2 ms of the readout pulse for initial $m_s = 0$ and $m_s = -1$ spin states. (c) Contrast as a function of ionization-pulse duration $t_{ion}$. (d, e) Photon number distributions $P(n)$ of $NV_A$ for the initial spin states $m_s = 0$ and $m_s = -1$ with the pristine (d) and the glycerol-coated surface (e). The optimal threshold photon number, $n_{th}$, for the distributions is indicated.

pulse duration $t_{ion}$. The SCC readout contrast $C = 1 - \alpha_0/\alpha_{-1}$ is plotted in Figure 3c. The maximum contrast $C_{max} \approx 32\%$ is found with an optimal $t_{ion} \approx 50$ ns. Similar to the mechanism of standard photoluminescence-based (PL) readout (Supporting Information), the achievable contrast in SCC is limited by the spin-dependent intersystem crossing rates (Supporting Information). With further increasing $t_{ion}$, the spin contrast decreases due to the relaxation of the singlet-state population back to the ground state and vanishes at $t_{ion} \approx 300$ ns, the approximate singlet-state lifetime. The spin-readout contrast with the glycerol-coated surface is similar to the value obtained with the pristine surface condition.

The $m_s$-dependent photon-number distributions for $NV_A$ are plotted in Figure 3d,e for the pristine (d) and the glycerol-coated (e) surface, from which we extracted the respective $NV^-$ population $\tilde{p}_{m_s}$.[11,14] While for the pristine surface, the difference $\tilde{p}_{-1} - \tilde{p}_0 \approx 0.145$, the value increases to $\approx 0.19$ after adding glycerol, which is a direct result of the charge-state stability improved with glycerol. However, in the SCC-based spin readout, the final charge state is determined by counting photons and assigning the charge/spin states based on a threshold photon number $n_{th}$.[16] The precision of assigning the correct charge and thus spin state depends on the distinguishability of the photon number distributions $P_{m_s}(n)$ for the initial spin states $m_s$. In order to quantify the improved distinguishability of $P_{m_s}(n)$ after coating the surface with glycerol, we

performed a Kolmogorov−Smirnov test that measures the maximum difference between the $m_s$-dependent cumulative photon distributions. The test yields values of 0.145 for the pristine surface and 0.174 for the glycerol-coated surface, an improvement of $\approx 20\%$. We note that no postselection of the data was applied to discard for example events executed in the $NV^0$ state.[19]

The improvement in distinguishability arises due to better mapping of the spin-states onto the charges state. We quantify the mapping efficiency as the population transfer from the initial spin state, which is $P_0(NV^-)$ assuming an ideal $\pi$ pulse, to the population in the charge states $\tilde{p}_{-,0}$:

$$\eta = \frac{\tilde{p}_{-,0} - P_0(NV^-)}{P_0(NV^-)} \tag{1}$$

The mapping efficiencies for $NV_A$ to $NV_D$ are shown in Figure 4. For mapping $m_s = 0$ to $NV^0$, a modest improvement
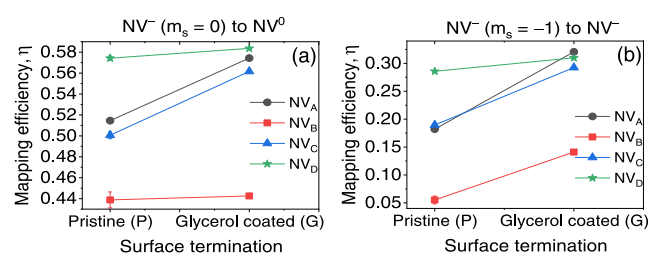


**Figure 4.** Effect of diamond surface termination on the efficiency of spin-state-dependent charge state mapping. The mapping efficiency for $m_s = 0$ to $NV^0$ (a) and $m_s = -1$ to $NV^-$ (b). Glycerol coating improves the spin-to-charge conversion efficiency, irrespective of the initial spin state of the $NV^-$ center.

is seen when glycerol is applied (Figure 4a). The mapping efficiency for $m_s = -1$ to $NV^-$ (Figure 4b) increases drastically when glycerol is applied to the surface and is around 50% for $NV_A$. The difference in improving the mapping efficiency for different spin states is not obvious, and an understanding of this observation requires further investigation that involves time dynamics and transition rates between various states. One can also see from the plots in Figure 4 that for $NV_D$, which was already stable with the pristine surface, addition of glycerol does not change much its charge-state mapping, while the efficiency for emitters with unstable charge environment benefits from surface passivation. Thus, different NV centers might experience different effects of adding glycerol coating, which is eventually determined by the overall charge environment of the center.

For a set $n_{th}$ the spin-readout noise can be calculated via[14]

$$\sigma_R^{SCC}(t_R) = \sqrt{(p_0 + p_{-1})(2 - p_0 - p_{-1})/(p_0 - p_{-1})^2} \tag{2}$$

where $p_0$ and $p_{-1}$ are the probabilities for the initial spin states $m_s = 0$ and $m_s = -1$ to measure $NV^-$ at time $t_R$ during the readout step, respectively. Extracted from the distributions $P_{m_s}(n)$, in Figure 5a we plot $\sigma_R^{SCC}(t_R)$ for $NV_A$ for both the pristine and the glycerol-coated surface. With increasing $t_R$, more photons are accumulated, and the confidence for assigning the correct spin state improves. Hence, $\sigma_R^{SCC}(t_R)$ decreases to an optimal value. For longer $t_R$, charge-state switching occurs, thus causing uncertainty in determining the correct spin state and increasing $\sigma_R^{SCC}(t_R)$. With the glycerol-covered surface, $\sigma_R^{SCC}(t_R)$ is higher initially due to generally
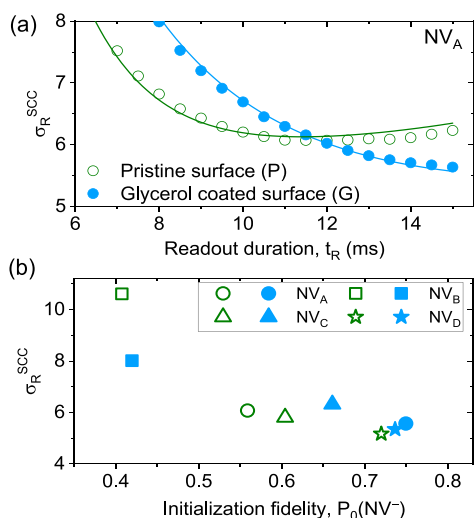
**Figure 5.** Charge-initialization probability and spin-readout noise. (a) Measured spin-readout noise $\sigma_R^{SCC}$ for $NV_A$ versus readout duration $t_R$. The symbols are calculated from the measured distributions (cf. Figures 3d and 3e), and the solid lines are calculated from the extracted rates. (b) Optimal $\sigma_R^{SCC}$ obtained within $t_R < 15$ ms readout time versus charge-initialization probability $P_0(NV^-)$ for $NV_A-NV_D$. The green and blue symbols represent measured values with the pristine and glycerol-coated surface, respectively. The impact of glycerol coating on $\sigma_R^{SCC}$ is substantial for the charge-unstable NV center, $NV_B$, while others show no improvement within $t_R < 15$ ms as a result of lower photon counts. The optimal values of $\sigma_R^{SCC}$ together with the corresponding $t_R$ values obtained via simulation of the readout process for the glycerol-coated surface are summarized in Table 1.

lower photon counts, and the optimal $\sigma_R^{SCC}(t_R)$ is obtained at later times as a result of the improved charge-state stability.

Figure 5b illustrates the optimal $\sigma_R^{SCC}(t_R)$ versus the charge initialization probability for $NV_A-NV_D$ obtained within a maximum readout time $t_R = 15$ ms. It is evident that the readout noise improves with increasing $P_0(NV^-)$, decreasing $\Gamma^{-0}$ (see Figure 2a) irrespective of the surface condition. The readout noise is higher for the charge-unstable NV centers (e.g., $NV_B$), and the improvement upon application of glycerol is significant. The influence of glycerol on $\sigma_R^{SCC}$ is minimal for the NV centers that are charge stable already with the pristine surface (e.g., $NV_C$ and $NV_D$). All key parameters for $NV_A-NV_D$ are summarized in Table 1, for both the pristine (P) and the glycerol-covered (G) surface. In the experiments, the maximum readout duration $t_R$ was 15 ms. However, the significantly reduced $\Gamma^{-0}$ after adding glycerol enables extended measurement times $t_R > 15$ ms. We thus simulated the measurement process (see the Supporting Information) to

extract the optimal $t_R$ and $n_{th}$ that minimizes $\sigma_R^{SCC}$ globally. It is clear that for all four NV centers and due to decreased $\Gamma^{-0}$, glycerol allows for extended measurement times $t_R > 15$ ms as compared to the pristine surface. The minimum readout noise we obtain is $\approx 5\ \sigma_p$ at $t_R \approx 12.8$ ms for $NV_D$ with $P_0(NV^-) \approx 0.75$ and the pristine surface. This result is comparable to the readout noise previously obtained with a shallow NV center in a nanopillar[26] with significantly higher photon counts. We note that with the diamond sample turned over and the NV centers adjacent to the immersion oil with higher photon counts, we obtain a readout noise as low as $\approx 3.5\sigma_p$. The relation between $\sigma_R$, $t_R$, and bandwidth normalized sensitivity will be addressed in the following section.

## ■ DISCUSSION

Deuterated glycerol not only increases the spin coherence of near-surface NV centers as shown previously,[34] but it generally improves the initialization probability $P_0(NV^-)$ into the negative charge state and reduces the ionization rate $\Gamma^{-0}$ from $NV^-$ to $NV^0$. Our sample preparation routine with triacid cleaning only yields a partial surface termination with oxygen. Hence, the general improvement of the NV charge properties with glycerol could be assigned to the passivation of surface-related charges and traps.[10,11] It is, however, also possible that glycerol lowers the Fermi level outside the diamond, reducing the effect of energy-band bending and thus improving the charge stability of $NV^-$.[25,35] Irrespective of the physical mechanism, our findings highlight the influence of the surface-related charge environment on $P_0(NV^-)$ as well as $\Gamma^{-0}$ during the readout with a weakly selective 594 nm laser.

In the following, we discuss the application of SCC in the context of a realistic sensing sequence and compare it to the standard PL readout. The flat sample geometry, although practical, in our case limits the photon counts to approximately 65K counts/s with 532 nm excitation at saturation. With PL spin readout in a 1 $\mu$s window, we thus obtain $\sigma_R^{PL} \approx 30\sigma_p$, a factor of 6 higher than the lowest $\sigma_R^{SCC} \approx 5.2\sigma_p$ we obtained for $NV_D$. Our results demonstrate that even with a pristine surface, it is feasible to locate charge-stable NV centers, implanted $\approx 5$ nm deep, for which $\sigma_{R,min}^{SCC}$ is comparable to values previously only obtained from NV centers in nanobeams or deep inside bulk diamonds. However, the flat sample geometry as applied here and, although practical, limits the attainable photon count rate. To minimize $\sigma_R^{SCC}$, the $t_R$ is thus required to be of the order of several milliseconds to collect a sufficient number of photons. These optimal times are even longer with the glycerol-coated surface, as the photon collection efficiency is further reduced. To account for the variability in the measurement overhead, we estimate the sensitivity to magnetic fields $\eta \propto \sigma_R(t_R)\sqrt{(\tau + t_I + t_R)/\tau^2}$,[14] where $\tau$, $t_I$, and $t_R$ are

**Table 1. Summary of the Key Parameters Measured and Simulated for $NV_A-NV_D$ for the Pristine (P) and the Glycerol-Coated (G) Surface Condition**[a]

| | $P_0(NV^-)$ | | $\Gamma^{-0}$ (Hz) | | $\sigma_R^{SCC}$ ($\sigma_p$) (measured) | | $\sigma_R^{SCC}$ ($\sigma_p$) (simulated) | | $n_{th}$ (measured) | | $n_{th}$ (simulated) | | $t_R$ (ms) (measured) | | $t_R$ (ms) (simulated) | |
| --- | --- | --- | --- | --- | --- | --- | --- | --- | --- | --- | --- | --- | --- | --- | --- | --- |
| | P | G | P | G | P | G | P | G | P | G | P | G | P | G | P | G |
| $NV_A$ | 0.56 | 0.75 | 101 | 9 | 6.0 | 5.6 | 6.1 | 4.6 | 7 | 4 | 6 | 11 | 10.4 | 14.9 | 8.7 | 55.9 |
| $NV_B$ | 0.42 | 0.52 | 157 | 104 | 10.7 | 8.2 | 10.6 | 4.8 | 3 | 3 | 3 | 16 | 4.3 | 14.9 | 3.8 | 138 |
| $NV_C$ | 0.60 | 0.66 | 74 | 16 | 5.8 | 6.1 | 5.8 | 6.2 | 7 | 5 | 8 | 6 | 10.9 | 15 | 12.6 | 21.3 |
| $NV_D$ | 0.72 | 0.74 | 23 | 8 | 5.2 | 5.4 | 5.2 | 4.8 | 8 | 4 | 7 | 9 | 12.8 | 15 | 11.2 | 49.4 |

[a]The uncertainty in $\sigma_R$ is around $0.1\sigma_p$.

the interrogation, the initialization, and the readout times, respectively. Considering a similar initialization-pulse duration of 1 $\mu$s, and an optimal readout duration for PL (1 $\mu$s) and SCC (12 ms for $NV_A$ with the pristine surface) minimizing $\sigma_R$, we obtain $\eta_{SCC} < \eta_{PL}$ for $\tau > 500$ $\mu$s. Despite the improved charge stability, for the glycerol-covered surface the required $\tau$ would even be longer due to the further increased $t_R$ as a result of decreased photon counts compared to the pristine surface. The increased distance to the potential sensing medium due to the glycerol layer thickness currently poses an additional challenge. For relaxometry measurements that are conducted on time scales $T_1 \approx 1$ ms, with our system parameters, SCC thus would have an advantage compared to PL readout. The interrogation times $\tau > 500$ $\mu$s required for SCC to be beneficial are much longer than the $T_2$ coherence times (3−15 $\mu$s) measured for the shallow NV centers in our sample. Increasing $T_2$ beyond 500 $\mu$s by applying higher-order dynamical-decoupling sequences,[36] by coherently driving bath spins in the NV environment,[37,38] or via application of a concatenated driving schemes[39,40] is challenging and remains to be explored experimentally. We thus anticipate that for the implementation of $T_1$-relaxometry sensing schemes on shallow NV centers with the pristine surface, it is advantageous to use the SCC instead of the PL readout. The minimum interrogation time beyond which SCC is beneficial can be further decreased by improving the photon collection via application of suitable photonic structures[7,8] increasing the photon count rate.

The spin-to-charge readout may also be applied in the context of quantum information processing with NV centers in diamonds at room temperature. In combination with a photoelectric readout, the spin-to-charge mapping with charge state readout has the potential of NV center spin state readout with high spatial resolution.[9] Here a figure of merit is the single spin readout fidelity $\mathcal{F}$, which should be >0.79 for single-shot readout with SNR > 1.[16] In our experiment, for $NV_D$ the readout fidelity is ~0.58 and ~0.61 with the pristine and glycerol-coated surface, respectively.

## CONCLUSION AND OUTLOOK

In summary, in this article we investigated the charge-state stability of single NV centers implanted with a mean depth $\approx 5$ nm below the surface of a flat diamond sample. Applying standard processing and surface preparation by means of triacid cleaning,[28] we observe a strong variation in the probability for initializing the NV centers into the negative charge state. The $NV^-$ charge-state initialization probability increases for all investigated NV centers after coating the diamond surface with glycerol and reaches up to $\approx 75\%$ which is comparable to NV centers deep in the bulk. Our observations thus demonstrate that deuterated glycerol does not only enhance the coherence time of near-surface NV centers[34] but also improves the initialization probability and stability of the negative-charge state $NV^-$. While the role of surface electron traps on charge-state stability[10,11,41] and their detrimental effects on spin-based measurement protocols are recognized,[11,42] the exact physical mechanism of our observations is not entirely clear. We hypothesize that the observations may also be explained by a reduction of the effect of energy-band bending via a change of the local electric-field potential. Further investigations are thus required, including surface electron spectroscopy,[43] electrical manipulation via

application of a gate voltage,[44] and variation of different oxygen and hydrogen surface terminations.[25]

We demonstrate the SCC protocol for shallow NV centers, obtaining a minimum readout-noise figure $\sigma_R^{SCC}$ in the range $5\sigma_p$ to $6\sigma_p$, a substantial reduction compared to standard PL readout with $\sigma_R^{PL} \approx 35\sigma_p$. However, the reduction in $\sigma_R$ is achieved at the cost of substantially increased readout times. Previously, SCC has only been achieved with NV centers located far from the diamond surface where surface-related charge instabilities are insignificant or in nanobeams with higher photon collection efficiency. For NV centers where glycerol significantly lowers the ionization rate, thus improving charge stability during readout, we observe an improvement of $\sigma_R^{SCC}$ as prolonged readout times are allowed. However, the low photon count rate, limited by our sample configuration, requires extended readout times with the optimum $t_R > 4$ ms. With our configuration presented here, an improvement in terms of sensitivity is thus achieved for measurement sequences with an interrogation time $\tau > 500$ $\mu$s, currently comprising relaxometry. The achievable interrogation times with dynamical decoupling and concatenated driving schemes remain to be explored. We expect that the optimal readout times can substantially be lowered by increasing the photon collection efficiency, reducing $t_R$ and yielding a benefit of SCC for interrogation times <500 $\mu$s.

We envision our findings will motivate further investigations on the surface functionalization and charge state dynamics of shallow NV centers and potentially the application of the SCC protocol for near-surface NV centers with improved noise figures compared to standard PL readout. Structuring the diamond with, for example, nanopillars will enhance the photon collection efficiency, thus improving the sensitivity even further for shorter interrogation times. Finally, we would like to note that despite the long readout times, SCC can be the enabling technique such as in recently demonstrated covariance magnetometry.[20]

## ASSOCIATED CONTENT

**Ⓢ Supporting Information**

The Supporting Information is available free of charge at https://pubs.acs.org/doi/10.1021/acsaelm.3c01141.

Details of the experimental protocols, optimization of the laser pulses for the SCC protocol, estimation of the optimal readout duration to minimize the SCC-based spin-readout noise (PDF)

## AUTHOR INFORMATION

### Corresponding Authors

**Rakshyakar Giri** − *Center for Macroscopic Quantum States (bigQ), Department of Physics, Technical University of Denmark, 2800 Kgs. Lyngby, Denmark;* ⓘ orcid.org/0000-0003-4576-8921; Email: ragiri@dtu.dk

**Alexander Huck** − *Center for Macroscopic Quantum States (bigQ), Department of Physics, Technical University of Denmark, 2800 Kgs. Lyngby, Denmark;* ⓘ orcid.org/0000-0002-2354-5922; Email: alhu@dtu.dk

### Authors

**Rasmus Høy Jensen** − *Center for Macroscopic Quantum States (bigQ), Department of Physics, Technical University of Denmark, 2800 Kgs. Lyngby, Denmark*

**Deepak Khurana** − *Center for Macroscopic Quantum States (bigQ), Department of Physics, Technical University of Denmark, 2800 Kgs. Lyngby, Denmark*

**Juanita Bocquel** − *Center for Macroscopic Quantum States (bigQ), Department of Physics, Technical University of Denmark, 2800 Kgs. Lyngby, Denmark*

**Ilya P. Radko** − *Center for Macroscopic Quantum States (bigQ), Department of Physics, Technical University of Denmark, 2800 Kgs. Lyngby, Denmark;* orcid.org/0000-0002-5929-1899

**Johannes Lang** − *Institute for Quantum Optics and Center for Integrated Quantum Science and Technology (IQST), Ulm University, 89081 Ulm, Germany*

**Christian Osterkamp** − *Institute for Quantum Optics and Center for Integrated Quantum Science and Technology (IQST), Ulm University, 89081 Ulm, Germany*

**Fedor Jelezko** − *Institute for Quantum Optics and Center for Integrated Quantum Science and Technology (IQST), Ulm University, 89081 Ulm, Germany*

**Kirstine Berg-Sørensen** − *Department of Health Technology, Technical University of Denmark, 2800 Kgs. Lyngby, Denmark*

**Ulrik L. Andersen** − *Center for Macroscopic Quantum States (bigQ), Department of Physics, Technical University of Denmark, 2800 Kgs. Lyngby, Denmark*

Complete contact information is available at:
https://pubs.acs.org/10.1021/acsaelm.3c01141

## Author Contributions

R.G. and R.H.J. contributed equally to this work.

## Notes

The authors declare no competing financial interest.

## ■ REFERENCES

(1) Taylor, J. M.; Cappellaro, P.; Childress, L.; Jiang, L.; Budker, D.; Hemmer, P. R.; Yacoby, A.; Walsworth, R.; Lukin, M. D. High-sensitivity diamond magnetometer with nanoscale resolution. *Nat. Phys.* **2008**, *4*, 810−816.

(2) Balasubramanian, G.; Chan, I. Y.; Kolesov, R.; Al-Hmoud, M.; Tisler, J.; Shin, C.; Kim, C.; Wojcik, A.; Hemmer, P. R.; Krueger, A.; Hanke, T.; Leitenstorfer, A.; Bratschitsch, R.; Jelezko, F.; Wrachtrup, J. Nanoscale imaging magnetometry with diamond spins under ambient conditions. *Nature* **2008**, *455*, 648−651.

(3) Dolde, F.; Fedder, H.; Doherty, M. W.; Nöbauer, T.; Rempp, F.; Balasubramanian, G.; Wolf, T.; Reinhard, F.; Hollenberg, L. C. L.; Jelezko, F.; Wrachtrup, J. Electric-field sensing using single diamond spins. *Nat. Phys.* **2011**, *7*, 459−463.

(4) Doherty, M. W.; Manson, N. B.; Delaney, P.; Jelezko, F.; Wrachtrup, J.; Hollenberg, L. C. The nitrogen-vacancy colour centre in diamond. *Phys. Rep.* **2013**, *528*, 1−45.

(5) Steiner, M.; Neumann, P.; Beck, J.; Jelezko, F.; Wrachtrup, J. Universal enhancement of the optical readout fidelity of single electron spins at nitrogen-vacancy centers in diamond. *Phys. Rev. B* **2010**, *81*, No. 035205.

(6) Jiang, L.; Hodges, J. S.; Maze, J. R.; Maurer, P.; Taylor, J. M.; Cory, D. G.; Hemmer, P. R.; Walsworth, R. L.; Yacoby, A.; Zibrov, A. S.; Lukin, M. D. Repetitive Readout of a Single Electronic Spin via Quantum Logic with Nuclear Spin Ancillae. *Science* **2009**, *326*, 267−272.

(7) Hedrich, N.; Rohner, D.; Batzer, M.; Maletinsky, P.; Shields, B. J. Parabolic Diamond Scanning Probes for Single-Spin Magnetic Field Imaging. *Phys. Rev. Applied* **2020**, *14*, No. 064007.

(8) Wildanger, D.; Patton, B. R.; Schill, H.; Marseglia, L.; Hadden, J. P.; Knauer, S.; Schönle, A.; Rarity, J. G.; O'Brien, J. L.; Hell, S. W.; Smith, J. M. Solid Immersion Facilitates Fluorescence Microscopy with Nanometer Resolution and Sub-Angstrom Emitter Localization. *Adv. Mater.* **2012**, *24*, OP309−OP313.

(9) Siyushev, P.; Nesladek, M.; Bourgeois, E.; Gulka, M.; Hruby, J.; Yamamoto, T.; Trupke, M.; Teraji, T.; Isoya, J.; Jelezko, F. Photoelectrical imaging and coherent spin-state readout of single nitrogen-vacancy centers in diamond. *Science* **2019**, *363*, 728−731.

(10) Dhomkar, S.; Jayakumar, H.; Zangara, P. R.; Meriles, C. A. Charge Dynamics in near-Surface, Variable-Density Ensembles of Nitrogen-Vacancy Centers in Diamond. *Nano Lett.* **2018**, *18*, 4046−4052.

(11) Bluvstein, D.; Zhang, Z.; Jayich, A. C. B. Identifying and Mitigating Charge Instabilities in Shallow Diamond Nitrogen-Vacancy Centers. *Phys. Rev. Lett.* **2019**, *122*, No. 076101.

(12) Gorrini, F.; Dorigoni, C.; Olivares-Postigo, D.; Giri, R.; Aprà, P.; Picollo, F.; Bifone, A. Long-Lived Ensembles of Shallow NV⁻ Centers in Flat and Nanostructured Diamonds by Photo-conversion. *ACS Appl. Mater. Interfaces* **2021**, *13*, 43221−43232.

(13) Aslam, N.; Waldherr, G.; Neumann, P.; Jelezko, F.; Wrachtrup, J. Photo-induced ionization dynamics of the nitrogen vacancy defect in diamond investigated by single-shot charge state detection. *New J. Phys.* **2013**, *15*, No. 013064.

(14) Shields, B. J.; Unterreithmeier, Q. P.; de Leon, N. P.; Park, H.; Lukin, M. D. Efficient readout of a single spin state in diamond via spin-to-charge conversion. *Phys. Rev. Lett.* **2015**, *114*, 136402.

(15) Manson, N.; Harrison, J. Photo-ionization of the nitrogen-vacancy center in diamond. *Diamond Relat. Mater.* **2005**, *14*, 1705−1710.

(16) Hopper, D. A.; Shulevitz, H. J.; Bassett, L. C. Spin Readout Techniques of the Nitrogen-Vacancy Center in Diamond. *Micromachines (Basel)* **2018**, *9*, 437.

(17) Hopper, D. A.; Grote, R. R.; Parks, S. M.; Bassett, L. C. Amplified Sensitivity of Nitrogen-Vacancy Spins in Nanodiamonds Using All-Optical Charge Readout. *ACS Nano* **2018**, *12*, 4678.

(18) Jayakumar, H.; Dhomkar, S.; Henshaw, J.; Meriles, C. A. Spin readout via spin-to-charge conversion in bulk diamond nitrogen-vacancy ensembles. *Appl. Phys. Lett.* **2018**, *113*, 122404.

(19) Jaskula, J. C.; Shields, B. J.; Bauch, E.; Lukin, M. D.; Trifonov, A. S.; Walsworth, R. L. Improved Quantum Sensing with a Single Solid-State Spin via Spin-to-Charge Conversion. *Physical Review Applied* **2019**, *11*, No. 064003.

(20) Rovny, J.; Yuan, Z.; Fitzpatrick, M.; Abdalla, A. I.; Futamura, L.; Fox, C.; Cambria, M. C.; Kolkowitz, S.; de Leon, N. P. Nanoscale covariance magnetometry with diamond quantum sensors. *Science* **2022**, *378*, 1301−1305.

(21) Mamin, H. J.; Kim, M.; Sherwood, M. H.; Rettner, C. T.; Ohno, K.; Awschalom, D. D.; Rugar, D. Nanoscale nuclear magnetic resonance with a nitrogen-vacancy spin sensor. *Science* **2013**, *339*, 557−60.

(22) Staudacher, T.; Shi, F.; Pezzagna, S.; Meijer, J.; Du, J.; Meriles, C. A.; Reinhard, F.; Wrachtrup, J. Nuclear Magnetic Resonance Spectroscopy on a (5-Nanometer)³ Sample Volume. *Science* **2013**, *339*, 561−563.

(23) Perona Martinez, F.; Nusantara, A. C.; Chipaux, M.; Padamati, S. K.; Schirhagl, R. Nanodiamond Relaxometry-Based Detection of Free-Radical Species When Produced in Chemical Reactions in Biologically Relevant Conditions. *ACS Sens.* **2020**, *5*, 3862−3869.

(24) Muller, C.; Kong, X.; Cai, J. M.; Melentijevic, K.; Stacey, A.; Markham, M.; Twitchen, D.; Isoya, J.; Pezzagna, S.; Meijer, J.; Du, J. F.; Plenio, M. B.; Naydenov, B.; McGuinness, L. P.; Jelezko, F. Nuclear magnetic resonance spectroscopy with single spin sensitivity. *Nat. Commun.* **2014**, *5*, 4703.

(25) Hauf, M. V.; Grotz, B.; Naydenov, B.; Dankerl, M.; Pezzagna, S.; Meijer, J.; Jelezko, F.; Wrachtrup, J.; Stutzmann, M.; Reinhard, F.; Garrido, J. A. Chemical control of the charge state of nitrogen-vacancy centers in diamond. *Phys. Rev. B* **2011**, *83*, No. 081304.

(26) Ariyaratne, A.; Bluvstein, D.; Myers, B. A.; Jayich, A. C. B. Nanoscale electrical conductivity imaging using a nitrogen-vacancy center in diamond. *Nat. Commun.* **2018**, *9*, 2406.

(27) Lang, J.; Häußler, S.; Fuhrmann, J.; Waltrich, R.; Laddha, S.; Scharpf, J.; Kubanek, A.; Naydenov, B.; Jelezko, F. Long optical coherence times of shallow-implanted, negatively charged silicon vacancy centers in diamond. *Appl. Phys. Lett.* **2020**, *116*, No. 064001.

(28) Brown, K. J.; Chartier, E.; Sweet, E. M.; Hopper, D. A.; Bassett, L. C. Cleaning diamond surfaces using boiling acid treatment in a standard laboratory chemical hood. *Journal of Chemical Health & Safety* **2019**, *26*, 40−44.

(29) Salvadori, M.; Araújo, W.; Teixeira, F.; Cattani, M.; Pasquarelli, A.; Oks, E.; Brown, I. Termination of diamond surfaces with hydrogen, oxygen and fluorine using a small, simple plasma gun. *Diamond Relat. Mater.* **2010**, *19*, 324−328.

(30) Cui, S.; Hu, E. L. Increased negatively charged nitrogen-vacancy centers in fluorinated diamond. *Appl. Phys. Lett.* **2013**, *103*, No. 051603.

(31) Findler, C.; Lang, J.; Osterkamp, C.; Nesládek, M.; Jelezko, F. Indirect overgrowth as a synthesis route for superior diamond nano sensors. *Sci. Rep.* **2020**, *10*, 22404.

(32) Hacquebard, L.; Childress, L. Charge-state dynamics during excitation and depletion of the nitrogen-vacancy center in diamond. *Phys. Rev. A* **2018**, *97*, No. 063408.

(33) Waldherr, G.; Beck, J.; Steiner, M.; Neumann, P.; Gali, A.; Frauenheim, T.; Jelezko, F.; Wrachtrup, J. Dark States of Single Nitrogen-Vacancy Centers in Diamond Unraveled by Single Shot NMR. *Phys. Rev. Lett.* **2011**, *106*, 157601.

(34) Kim, M.; Mamin, H. J.; Sherwood, M. H.; Ohno, K.; Awschalom, D. D.; Rugar, D. Decoherence of Near-Surface Nitrogen-Vacancy Centers Due to Electric Field Noise. *Phys. Rev. Lett.* **2015**, *115*, No. 087602.

(35) Karaveli, S.; Gaathon, O.; Wolcott, A.; Sakakibara, R.; Shemesh, O. A.; Peterka, D. S.; Boyden, E. S.; Owen, J. S.; Yuste, R.; Englund, D. Modulation of nitrogen vacancy charge state and fluorescence in nanodiamonds using electrochemical potential. *Proc. Natl. Acad. Sci. U. S. A.* **2016**, *113*, 3938−3943.

(36) Viola, L.; Knill, E.; Lloyd, S. Dynamical Decoupling of Open Quantum Systems. *Phys. Rev. Lett.* **1999**, *82*, 2417−2421.

(37) Bluvstein, D.; Zhang, Z.; McLellan, C. A.; Williams, N. R.; Jayich, A. C. B. Extending the Quantum Coherence of a Near-Surface Qubit by Coherently Driving the Paramagnetic Surface Environment. *Phys. Rev. Lett.* **2019**, *123*, 146804.

(38) Bauch, E.; Hart, C. A.; Schloss, J. M.; Turner, M. J.; Barry, J. F.; Kehayias, P.; Singh, S.; Walsworth, R. L. Ultralong Dephasing Times in Solid-State Spin Ensembles via Quantum Control. *Phys. Rev. X* **2018**, *8*, No. 031025.

(39) Cai, J.-M.; Naydenov, B.; Pfeiffer, R.; McGuinness, L. P.; Jahnke, K. D.; Jelezko, F.; Plenio, M. B.; Retzker, A. Robust dynamical decoupling with concatenated continuous driving. *New J. Phys.* **2012**, *14*, 113023.

(40) Stark, A.; Aharon, N.; Unden, T.; Louzon, D.; Huck, A.; Retzker, A.; Andersen, U. L.; Jelezko, F. Narrow-bandwidth sensing of high-frequency fields with continuous dynamical decoupling. *Nat. Commun.* **2017**, *8*, 1105.

(41) Stacey, A.; Dontschuk, N.; Chou, J.-P.; Broadway, D. A.; Schenk, A. K.; Sear, M. J.; Tetienne, J.-P.; Hoffman, A.; Prawer, S.; Pakes, C. I.; Tadich, A.; de Leon, N. P.; Gali, A.; Hollenberg, L. C. L. Evidence for Primal sp$^2$ Defects at the Diamond Surface: Candidates for Electron Trapping and Noise Sources. *Advanced Materials Interfaces* **2019**, *6*, 1801449.

(42) Giri, R.; Gorrini, F.; Dorigoni, C.; Avalos, C. E.; Cazzanelli, M.; Tambalo, S.; Bifone, A. Coupled charge and spin dynamics in high-density ensembles of nitrogen-vacancy centers in diamond. *Phys. Rev. B* **2018**, *98*, No. 045401.

(43) Sangtawesin, S.; et al. Origins of Diamond Surface Noise Probed by Correlating Single-Spin Measurements with Surface Spectroscopy. *Phys. Rev. X* **2019**, *9*, No. 031052.

(44) Grotz, B.; Hauf, M. V.; Dankerl, M.; Naydenov, B.; Pezzagna, S.; Meijer, J.; Jelezko, F.; Wrachtrup, J.; Stutzmann, M.; Reinhard, F.; Garrido, J. A. Charge state manipulation of qubits in diamond. *Nat. Commun.* **2012**, *3*, 729.